A&A 635, L13 (2020)
https://doi.org/10.1051/0004-6361/201937137
© ESO 2020

Astronomy & Astrophysics

LETTER TO THE EDITOR

Lithium-rotation connection in the newly discovered young stellar stream Psc–Eri (Meingast 1)⋆

J. Arancibia-Silva[1,2], J. Bouvier[3], A. Bayo[1,2], P. A. B. Galli[4], W. Brandner[5], H. Bouy[4], and D. Barrado[6]

[1] Instituto de Física y Astronomía, Universidad de Valparaíso, Valparaíso, Chile
e-mail: javier.arancibia@postgrado.uv.cl
[2] Núcleo Milenio Formación Planetaria – NPF, Universidad de Valparaíso, Av. Gran Bretaña 1111, Valparaíso, Chile
[3] IPAG, Univ. Grenoble Alpes, 38000 Grenoble, France
[4] Laboratoire d'Astrophysique de Bordeaux, Univ. Bordeaux, CNRS, B18N, Allée Geoffroy Saint-Hilaire, 33615 Pessac, France
[5] Max Planck Institute for Astronomy, Heidelberg, Germany
[6] Depto. Astrofísica, Centro de Astrobiología (INTA-CSIC), ESAC Campus, Camino Bajo del Castillo s/n, 28692 Villanueva de la Cañada, Spain

Received 18 November 2019 Accepted 24 February 2020

ABSTRACT

Context. As a fragile element, lithium is a sensitive probe of physical processes occurring in stellar interiors.
Aims. We aim to investigate the relationship between lithium abundance and rotation rate in low-mass members of the newly discovered 125 Myr-old Psc–Eri stellar stream.
Methods. We obtained high-resolution optical spectra and measured the equivalent width of the 607.8 nm LiI line for 40 members of the Psc–Eri stream, whose rotational periods have been previously derived.
Results. We show that a tight correlation exists between the lithium content and rotation rate among the late-G to early-K-type stars of the Psc–Eri stream. Fast rotators are systematically Li rich, while slow rotators are Li depleted. This trend mimics that previously reported for the similar age Pleiades cluster.
Conclusions. The lithium-rotation connection thus seems to be universal over a restricted effective temperature range for low-mass stars at or close to the zero-age main sequence, and does not depend on environmental conditions.

Key words. stars: low-mass – stars: pre-main sequence – stars: abundances – open clusters and associations: individual: Psc–Eri – stars: rotation

1. Introduction

The evolution of lithium abundance over the lifetime of a star reflects transport processes operating in the stellar interior. Lithium, a fragile element that is burned at a temperature of 2.5 MK encountered at the base of the convective zone of low-mass stars, is slowly depleted and its surface abundance steadily decreases over time in solar-type and lower-mass stars (see, e.g., Jeffries 2014, for a review).

Li depletion is extremely dependent on temperature (e.g, Bildsten et al. 1997), making Li abundances a very sensitive diagnostic of the physics of transport processes in stellar interiors. More vigorous transport processes leads to more severe Li depletion. Beyond the dependence on temperature, Li depletion can also be affected by nonstandard transport processes, such as rotational mixing, internal magnetic fields, and by structural changes induced by, for instance, rotation, magnetic activity, metallicity, or accretion (e.g., Pinsonneault et al. 1990; Zahn 1992; Ventura et al. 1998; Piau & Turck-Chièze 2002; Talon & Charbonnel 2005; Denissenkov 2010; Eggenberger et al. 2012; Théado & Vauclair 2012). These additional mechanisms depend at the same time on initial conditions and evolutionary paths. It is therefore important to investigate lithium content in relation to other properties of the stars at different ages and in different environments.

A connection between lithium abundance and rotation has been reported in young stellar populations at different ages, where rapid rotators are found to have systematically higher Li abundances than slow rotators. This relationship is somewhat counterintuitive as rotational mixing is thought to scale with surface rotation, and would thus predict Li-depleted fast rotators. Soderblom et al. (1993) first reported this trend for the Pleiades (age ∼125 Myr), which was recently confirmed and extended by Bouvier et al. (2018). The Li-rotation connection was also investigated at such young ages as ∼5 Myr, in the case of NGC 2264 (Bouvier et al. 2016), and in the β Pic moving group at 20 Myr (Messina et al. 2016). Studying this relationship at different ages and/or in different environments is key to decipher its origin.

In this paper, we focus on studying this relationship in the newly discovered solar-metallicity ([Fe/H] = −0.04 ± 0.15) stellar stream Psc–Eri (Meingast et al. 2019) (Meingast 1 in Ratzenböck et al. 2020), which is similar in age to the Pleiades (Curtis et al. 2019), but is located in an overall very different environment. We combine our new lithium equivalent width (EW(Li)) measurements with the rotational periods reported by Curtis et al. (2019) to investigate the lithium-rotation connection in this new environment.

⋆ Based on observations collected at the European Organisation for Astronomical Research in the Southern Hemisphere under ESO programme 103.A-9009.

2. Methodology

2.1. Stellar sample

Our starting sample was that of candidate members listed by Curtis et al. (2019) who derived rotational periods from the Transiting Exoplanet Survey Satellite (TESS) light curves (Ricker et al. 2015). We additionally used Curtis et al. (2019) $T_{\rm eff}$ estimates, which are indistinguishable from *Gaia* DR2 values, to select members with $T_{\rm eff}$ in the range 4000–5500 K, corresponding to spectral type G5-K6. This is the $T_{\rm eff}$ range over which the relationship between lithium and rotation was observed in the Pleiades. We thus obtained a sample of 66 late-G and early- to mid-K-type stars in the Psc–Eri stream.

2.2. Observations

Among this initial sample, we observed 40 stars with the FEROS (Kaufer et al. 1999) high-resolution spectrograph ($R \sim 48\,000$) mounted at the ESO/MPG 2.2 m telescope at ESO/La Silla Observatory. The observations were obtained from July 24 to August 2, 2019, as part of Programme 103.A-9009. We observed the targets in object-calibration mode, which allows for the simultaneous acquisition of the object spectrum and the ThAr lamp. The exposure times ranged from 2 min to 25 min, depending on the magnitude of the target. We reduced the collected spectra with the FEROS data reduction pipeline which performs bias subtraction, flat-fielding, wavelength calibration, barycentric velocity correction, and merging of the extracted echelle orders into a single one-dimensional spectrum that we used in the forthcoming analysis. Most spectra have a signal-to-noise ratio (S/N) between 30 and 50. However, a couple of objects have low quality spectra, namely curt#92 ($S/N \sim 10$) and curt#43 ($S/N \sim 15$). Radial velocities ($V_{\rm r}$) were estimated via cross correlation with a synthetic K0 spectral mask to further correct the spectra and shift it to the rest frame (the values are summarized in Table 1). As a consequence of visibility and airmass constraints, 40 objects were observed out of the 66 from the previously described sample, however this subsample homogeneously covers the range of $T_{\rm eff}$ and rotational periods that we wanted to explore.

2.3. Lithium equivalent width measurements

We obtained EW(Li) using an automatic technique described in Appendix A of Bayo et al. (2011). In addition, we independently measured EW(Li) interactively from direct integration and Gaussian fitting using the IRAF/splot command. The comparison of the two methods yielded consistent results for most cases. A few discrepant cases resulted from low S/N spectra (Obj 15), bad pixels affecting the automatic continuum determination (Obj 94), or fast rotation leading to strong line blends (Obj 2, 34) that required special treatment.

For the three fast rotators curt#79, 88, 71, we estimated $v \sin i$ values of 55, 55, and 61 km s^{-1}, respectively, via the previously mentioned K0 mask cross-correlation. The broadening of the lines of these objects led us to consider the potential impact of line blends on the EW(Li) measurements. We applied the same method as that used for Pleiades fast rotators described in Bouvier et al. (2018, Paper I). Namely, we selected a slow rotator of the same spectral type, produced an artificial Gaussian LiI 6708 Å line in its spectrum, and rotationally broadened the spectrum to the $v \sin i$ of the fast rotator. We then measured EW(Li) in the broadened spectrum and compared it to the input value. As in Paper I, we find that the blends do not affect the EW(Li) measurements for these moderate $v \sin i$ values. As an additional check, we also used low $v \sin i$ Psc–Eri members of the same spectral type with varying degree of EW(Li), broadened their spectra, and used them as templates. For instance, Curt#46 is an intrinsically fast rotator with a period of 1.26 d but with moderate $v \sin i$ (21 km s^{-1}), presumably seen at low inclination. This object exhibits a deep and relatively narrow lithium line and is thus a good template to measure EW(Li) in the broadened spectra of other fast rotators. In most cases, this approach yielded similar results as the direct measurements in broadened spectra, which confirms that blends do not significantly affect the derived EW(Li), even for relatively high $v \sin i$ objects.

Finally, as in Paper I, we applied a correction on the measured equivalent width to account for the blend by the nearby FeI 6707.441 Å line. Following the prescription of Soderblom et al. (1993), we derived the intrinsic $(B-V)$ color of the targets from their $T_{\rm eff}$, interpolating through Pecaut & Mamajek (2013) $(B-V)$–$T_{\rm eff}$ relationship. Over the $(B-V)$ range of our sample, the FeI blend correction to EW(Li), which is listed in Table 1, amounts to 11–19 mÅ, and is thus comparable to our measurement errors. This correction has not been applied to EW(Li) upper limits. Having thus derived EW(Li) for all the objects in our sample, and using rotational periods and $T_{\rm eff}$ from Curtis et al. (2019), we are able to study the relationship between lithium and rotation for the low-mass members of the Psc–Eri stream.

3. Results

Before presenting the results of the lithium-rotation relationship for Psc–Eri members below, we discuss a few outliers in the Curtis et al. (2019) sample that required further analysis. Curtis et al. (2019) identified five "Slow" stars in their sample, i.e., stars that are lying significantly above the slow rotator sequence of the Psc–Eri stream. Two of these stars are included in our sample. Curt#49 is reported to have a 12.22 d period. The object has two TESS light curves in the MAST archive from Sectors 4 and 5. The first is of low quality and does not yield a period. The second exhibits a smooth modulation and a CLEAN periodogram analysis indicates a clear period of 6.083 d. We therefore adopted this value in the following, which brings this object back onto the slow rotator sequence. The other "Slow" object, Curt#92, has a reported period of 11.96 d. We queried the MAST archive for this object, but no processed TESS light curve is provided there. The closest object with a TESS light curve is 397 arcsec away. In any case, the S/N of the spectrum we obtained for this object, which is the poorest quality source in our campaign, $S/N \sim 10$, is too low to detect the lithium line in absorption. The uncertainty in the period and poor quality spectrum prompted us to discard this object in the following analysis.

Our preliminary analysis revealed another outlier in the lithium-rotation-$T_{\rm eff}$ plane, namely Curt#75 with a reported period of 1.93 d (Curtis et al. 2019), i.e., an intrinsically fast rotator. However, its spectrum exhibits narrow photospheric line profiles and no sign of lithium absorption. The observer at the telescope noticed that two objects were visible on the acquisition camera. Indeed, 2MASS K-band and SDSS2 images reveal an elongated object at this position, most likely a nearly equal-mass binary with a separation of a few arcseconds. With its 21 arcsec-wide pixels, the TESS light curve cannot resolve the system. The FEROS spectrum was obtained for only one of the components and we cannot ascertain that this is the component for which a

Table 1. Stellar sample properties from Curtis et al. (2019) and EW(Li) measurements.

Gaia DR2	Curt	RA(2000) hh:mm:ss	Dec(2000) dd:mm:ss	$T_{\rm eff}$ K	G mag	M_G mag	G_{bp}–G_{rp} mag	$P_{\rm rot}$ d	EW(FeI) mÅ	EW(Li) mÅ	rms mÅ	$V_{\rm r}$ km s^{-1}	$v \sin i$ km s^{-1}
2349094158814399104	79 (*)	00:47:18.0	−22:45:08.1	4585	10.929	6.051	6.051	1.3	17	202	10	29.36	55
4975223840046231424	81	00:47:38.5	−47:41:45.8	4551	11.514	6.985	6.985	5.8		<50		15.67	7
2355466790769878400	96	00:55:21.5	−21:24:03.7	4135	12.341	7.578	7.578	6.84		<30		17.63	<6
5029398079322118912	52 (*)	01:13:42.4	−31:11:39.6	5003	10.804	5.959	5.959	6.64	14	196	5	20.24	<6
4984094970441940864	101	01:21:49.7	−42:01:22.3	4113	12.731	8.099	8.099	5.45		<30		20.61	7
2484875735945832704	65	01:24:24.7	−03:16:39.0	4842	11.791	6.398	6.398	8.4	15	82	13	16.84	7
2491594263092190464	56	02:10:22.3	−03:50:56.7	4944	11.533	6.153	6.153	2.26	14	225	10	19.37	19
5117016378528360448	91	02:17:14.6	−27:16:41.9	4308	12.551	7.451	7.451	5.92		<30		21.65	8
5118895478259982336	90 (*)	02:26:07.0	−24:54:49.0	4431	11.728	6.658	6.658	5.61	18	31	5	21.83	10
2488721720245150336	87	02:26:53.3	−05:17:45.2	4444	12.485	7.198	7.198	5.2		<30		21.19	8
5129876953722430208	76	02:29:28.5	−20:12:16.8	4829	11.695	6.739	6.739	8.0	15	99	5	22.7	7
2496200774431287424	36 (*)	02:30:58.8	−03:03:04.9	5448	10.415	5.328	5.328	5.45	11	173	5	22.25	<6
5179037454333642240	64	02:39:10.9	−05:32:22.5	4859	11.765	6.373	6.373	6.42	15	125	5	19.23	8
5161117923061794688	74	02:59:52.0	−09:47:35.8	4800	12.063	6.639	6.639	5.45	15	184	10	20.44	8
5045955865443216640	40	03:00:46.9	−37:08:01.5	5434	10.323	5.363	5.363	3.9	11	198	10	21.91	<6
5159567164990031360	88 (*)	03:04:46.0	−12:16:57.9	4330	12.613	7.098	7.098	0.45	19	50	30	19.27	55
7324465427953664	61	03:05:14.1	+06:08:53.5	4947	12.043	6.247	6.247	4.4	14	195	10	18.61	10
5103353606523787008	46 (*)	03:18:03.8	−19:44:14.2	5077	10.473	5.227	5.227	1.26	13	242	5	20.41	25
5106733402188456320	71 (*)	03:24:25.2	−15:50:05.4	4944	11.517	6.197	6.197	0.62	14	245	10	40.06	61
5168681021169216896	29	03:29:30.3	−07:10:13.8	5478	10.827	5.204	5.204	5.32	11	168	5	20.78	8
3247412647814482816	80	03:32:30.9	−06:13:09.1	4714	12.327	6.898	6.898	6.66	16	34	10	22.87	8
5114686272872474880	69	03:47:25.8	−12:32:30.9	5006	12.634	6.55	6.55	9.0	14	61	15	20.15	7
4842810376267950464	38	03:47:56.3	−41:56:24.9	5355	10.762	5.383	5.383	5.7	12	143	5	18.75	<6
3243665031151732864	50	03:48:38.3	−06:41:52.6	5063	11.46	5.953	5.953	6.84	13	151	5	22.04	<6
3245140743257978496	43 (*)	03:54:01.0	−06:14:14.6	5344	11.146	5.434	5.434	5.66	12	193	15	21.7	8
3193528950192619648	41	03:57:04.0	−10:14:00.9	5270	11.297	5.534	5.534	5.54	12	195	5	20.88	<6
5083255496041631616	49	03:57:35.1	−24:28:42.2	5078	11.131	5.885	5.885	6.08	13	7	5	22.98	<6
5097262136011410944	62	03:58:54.7	−17:05:53.2	4899	11.649	6.311	6.311	7.58	14	105	5	22.45	7
5096891158212909312	59	04:12:46.0	−16:19:29.1	4907	11.994	6.187	6.187	3.68	14	255	10	21.25	13
4871041608622321664	60 (*)	04:28:28.9	−33:53:45.1	4924	11.63	6.037	6.037	6.5	14	215	10	21.21	7
2594993646533642496	67	22:31:13.9	−17:04:52.4	4829	11.934	6.451	6.451	6.1	15	174	10	9.96	<6
2402197409339616768	57 (*)	22:39:01.4	−18:52:55.7	4921	11.219	6.155	6.155	7.8	14	115	5	13.09	<6
2596395760081700608	53	22:39:53.5	−16:36:23.3	5065	11.508	5.994	5.994	6.97	13	126	5	10.75	7
2433715455609798784	70	23:36:52.1	−11:25:01.7	4810	11.737	6.442	6.442	6.3	15	214	10	14.66	8
2393862836322877952	66 (*)	23:40:37.5	−18:11:37.9	4734	11.485	6.472	6.472	7.7	16	99	10	16.88	7
2390974419276875776	72	23:48:32.4	−18:32:57.4	4706	11.583	6.618	6.618	6.5	16	123	10	17.14	8
2418664520110763520	63	23:49:55.1	−15:43:42.0	4917	11.607	6.396	6.396	2.94	14	215	10	16.87	15
2339984636258635136	77	23:56:53.7	−23:17:24.6	4545	11.475	6.765	6.765	8.35	17	22	5	15.8	7

Notes. (*)Bona fide binary systems (see Sect. 3 for details.)

TESS period has been reported. Indeed, the narrow line profiles seem inconsistent with fast rotation unless the system is seen at a low inclination. In the light of these uncertainties, we discarded this source from the analysis.

We are thus left with 38 objects with TESS periods reported by Curtis et al. (2019) and with EW(Li) measured on the FEROS spectra. The results are listed in Table 1. Of these, 7 appear to be photometric binaries (PBs) in the *Gaia* color-absolute magnitude diagram shown in Fig. 1. Objects Curt#46, 79, 90 are well above the single stream sequence, while Curt#43, 60, 71, 88 are slightly above. Owing to the high accuracy of *Gaia* data and the narrowness of the single star sequence, we classified the 7 stars as PBs. In addition to these, to further study possible multiplicity effects, we looked for signs of tight companions, i.e., spectroscopic binaries (SBs). To search for single line SBs (SB1), we compared our $V_{\rm r}$ determinations with those of *Gaia* DR2. Among the objects with good quality spectra, we found 5 (namely Curt#36, 52, 57, 66, 79) with differences in $V_{\rm r}$ determination above 5σ. In particular, Curt#79 and #71 have been classified by us as PBs and also potential SB1 (although the delta in $V_{\rm r}$ for Curt#71 is only at the 3σ level). To complete the SB search, we visually inspected the CCFs looking for signs of resolved SBs (SB2) but we did not find any obvious candidate. With this analysis in hand, the SB fraction estimated for this stream is consistent with that determined for loose associations of similar age (∼10%; Elliott et al. 2014).

Regarding multiplicity effects on Li measurements assuming all of PBs and SBs found (Curt#36, 43, 46, 52, 57, 60, 66, 71, 79, 88, 90) as bona fide binary systems, four of our candidate binaries are fast rotators with periods lower than 2 days, and the other seven are slower rotators, with periods between ∼ 5 and ∼ 8 days. The binary candidates are distributed over nearly the whole range of periods. They also are not uniformly Li rich or Li poor, but seem to follow the same tendency as the single stars (see filled diamonds in Fig. 2). This suggest that the trend that we are reporting in the lithium content is most probably tied to the rotation of the stars and not to their multiple nature.

Figure 2 illustrates the resulting relationship between lithium content and rotation among the late-G- and early-K-type stars of the Psc–Eri stream. As previously reported by Curtis et al. (2019), stars in this mass range exhibit a wide range of rotational periods. The same behavior is seen in the Pleiades cluster, and

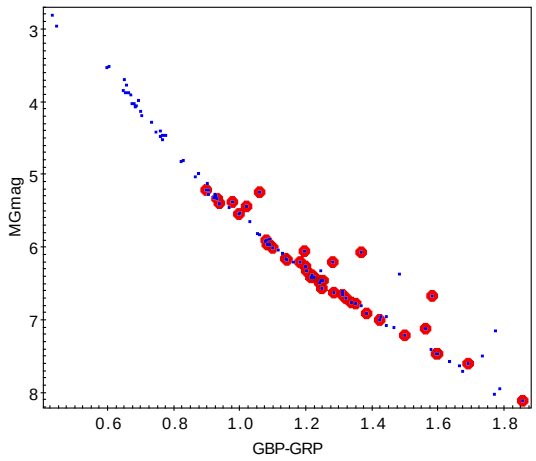

Fig. 1. Color-magnitude diagram from *Gaia* for the Psc–Eri sample. Small blue square: Curtis et al. (2019) sample. Large red circles: stars with lithium measurements from this study; 7 objects are located above the single star main sequence.

this is precisely this similarity that prompted Curtis et al. (2019) to assign the same age of 125 Myr to the Psc–Eri stream. The lithium measurements reported in this work also show a wide dispersion over this $T_{\rm eff}$ range, from undetectable ($\leq$30 mÅ) up to 260 mÅ. Assuming the same age and metallicity for the Psc–Eri stream as for the Pleiades, the latter value corresponds to a nearly pristine lithium abundance of A[Li] $\simeq$ 2.8 (see Bouvier et al. 2018).

Figure 2 very clearly reveals the dependence of lithium content on rotation rate at a given $T_{\rm eff}$, over the $T_{\rm eff}$ range from 4500 K to 5100 K. There, fast rotators with periods shorter than 4 d have EW(Li) ranging from 200 to 255 mÅ, while slow rotators with periods longer than 6 d exhibit lithium equivalent widths less than 215 mÅ down to undetectable levels ($\leq$30 mÅ), with a median value of 110 mÅ. As we previously found in the Pleiades cluster, there seems to be a tight lithium-rotation relationship that is valid for all stars over this $T_{\rm eff}$ range on the zero-age main sequence (ZAMS); slow rotators are lithium depleted compared to fast ones. Whether this relationship extends over a wider range of effective temperature awaits additional lithium measurements for both hotter and cooler stars of the stream.

4. Discussion and conclusions

Meingast et al. (2019) report a new, nearby stellar stream identified from the 6D position-velocity data provided by *Gaia* DR2. They estimate an age of 1 Gyr based on the location of member giant stars relative to model isochrones and derived a solar metallicity by cross-correlating their sample with LAMOST DR4. Curtis et al. (2019) derive rotational periods from TESS light curves for 101 low-mass members of the stream, that they named Psc–Eri. From the striking similarity of the rotation period versus mass diagrams of the Psc–Eri stream and of the Pleiades cluster, they assigned an age of 125 Myr to the former. Indeed, the distribution of rotation rates as a function of mass is quite sensitive to age, especially close to the ZAMS (e.g., Bouvier et al. 2014; Gallet & Bouvier 2015).

The connection we report between lithium and rotation for low-mass stars of the Psc–Eri stream is also strikingly similar to that reported earlier for the Pleiades cluster (Paper I). Fast rotators are systematically Li rich compared to slow rotators; this relationship is valid for single and binary systems over a limited $T_{\rm eff}$ range. This result when first reported by Soderblom et al. (1993) was somewhat unexpected. Most stellar evolution models would predict that faster rotators experience enhanced internal mixing and would thus burn lithium more efficiently (e.g., Pinsonneault et al. 1989). Fast rotators ought to be lithium depleted while the opposite was observed. Subsequent studies, including this work, unambiguously point to a higher lithium content in fast rotators at or close to the ZAMS. In Paper I, we summarized three classes of models that attempt to explain this paradoxical result and we only briefly recall these models in this Letter. Bouvier et al. (2016) provide a more extensive discussion of their success and limitations.

Bouvier (2008) related the lithium-rotation connection observed on the ZAMS to the pre-main sequence (PMS) rotational history of young solar-type stars. Current angular momentum evolution models predict that slow rotators remain locked to their circumstellar disk over a longer duration than fast rotators (e.g., Gallet & Bouvier 2015). As a result, a larger amount of internal differential rotation develops in slow rotators, which triggers enhanced mixing and leads to PMS Li depletion, while fast rotators maintain their original Li content (Eggenberger et al. 2012). Alternatively, Somers & Pinsonneault (2014, 2015) suggested that radius inflation in fast, magnetically active stars reduces PMS Li burning as a result of a lower temperature at the base of the convective zone. Assuming a relationship between rotation and magnetic activity during the PMS, the slow, more moderately active stars would not experience radius inflation and would thus start to deplete lithium earlier. Finally, Baraffe et al. (2017) argue that stellar rotation has a direct impact on the efficiency of internal transport processes and propose that fast rotation reduces the penetration of convective plumes into the radiative core, thus leading to a lower depletion rate in fast rotators. Any of these models, or combination of them, has the potential to explain the lithium-rotation connection reported in this work and in previous studies. Further studies will be needed to attempt to discriminate between the models.

The clear lithium-rotation relationship we report for the Psc–Eri low-mass members has two main implications. Firstly, the lithium-rotation connection seems to be universal for low-mass stars in a specific $T_{\rm eff}$ or mass range at or close to the ZAMS. This connection is reporteed in this work for the ZAMS stream Psc–Eri and has been previously reported in various star-forming regions, moving groups, and young open clusters with ages between 5 Myr and 125 Myr (Messina et al. 2016; Bouvier et al. 2016, 2018). Secondly, this relationship does not seem to be affected by environmental conditions. While the Psc–Eri stream and Pleiades cluster are probably similar in age (Curtis et al. 2019, Barrado et al., in prep.), they have different kinematic properties. The former is in the process of dissolving into the Galactic field, while the latter is still a well-defined young open cluster. Presumably, the Pleiades cluster formed from a very rich and dense environment, similar to the Orion Nebula Cluster (Kroupa et al. 2001), while the Psc–Eri stream may have originated from a rich albeit lower density OB or T association at birth. These different initial conditions have apparently had no impact on the lithium-rotation connection, whose origin is thus to be found in the physics of PMS stellar evolution. Further characterization of the lithium-rotation connection for stellar populations of different ages, metallicities, and environments will help to guide the development of PMS stellar evolution models able to account for this result.

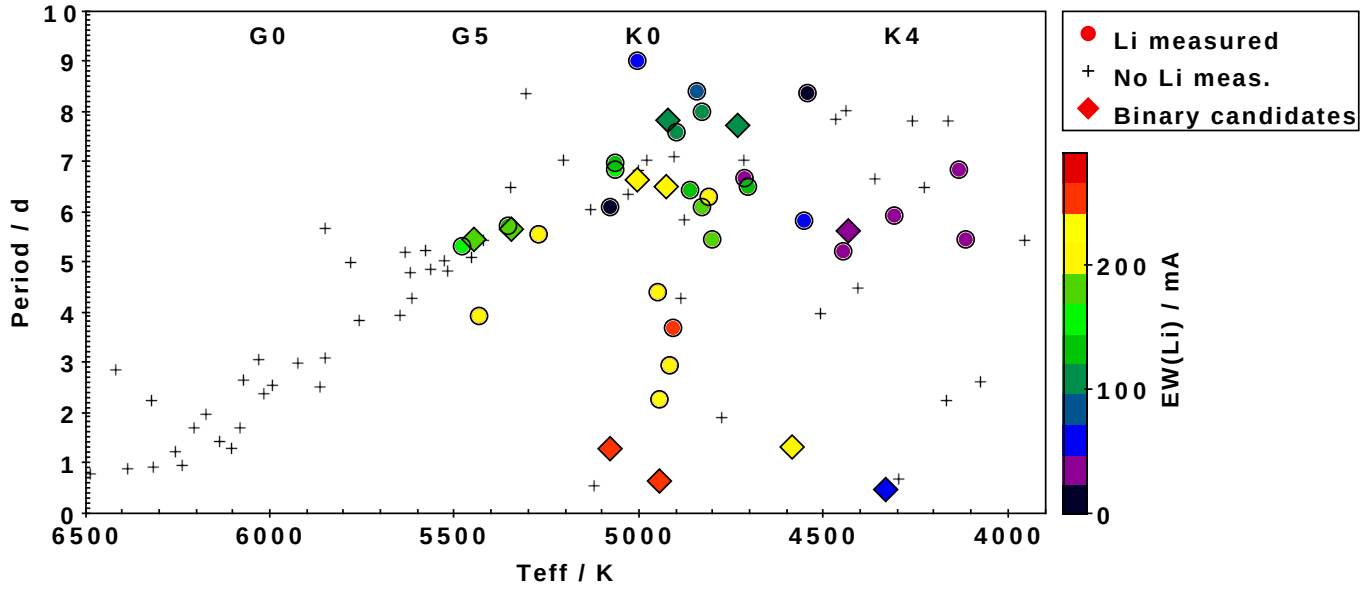

Fig. 2. Rotational period distribution of low-mass members of the Psc–Eri stream plotted as a function of effective temperature. Filled circles: stars with EW(LiI) measurements. The color code scales with EW(LiI). Crosses: stars without lithium measurements. Filled diamonds: bona fide binary systems.

Acknowledgements. AB and JB acknowledge funding from the ECOS 170006 – Conicyt C17U01 project for mutual visits. Most of this study was completed during a stay at University Valparaiso in the framework of this program. JA acknowledges finantial support from Universidad de Valparaíso via FIBUV grant. JA and AB acknowledge support from ICM (Iniciativa científica Milenio) via NPF; and from FONDECYT (grant 1190748). JB gratefully acknowledges the hospitality of IFA members during his visit. This research has received funding from the European Research Council (ERC) under the European Union's Horizon 2020 research and innovation programme (grant agreements No. 742095 SPIDI: Star-Planets-Inner Disk-Interactions, http://spidi-eu.org; and No. 682903, P.I.H. Bouy, COSMIC DANCE, http://astrophy.u-bordeaux.fr/en/cosmic-dance/), and from the French State in the framework of the "Investments for the future" Program, IdEx Bordeaux, reference ANR-10-IDEX-03-02. This research has been partially funded by the Spanish State Research Agency (AEI) Projects No. ESP2017-87676-C5-1-R and No. MDM-2017-0737 Unidad de Excelencia "María de Maeztu" – Centro de Astrobiología (INTA-CSIC).

References

Baraffe, I., Pratt, J., Goffrey, T., et al. 2017, ApJ, 845, L6
Bayo, A., Barrado, D., Stauffer, J., et al. 2011, A&A, 536, A63
Bildsten, L., Brown, E. F., Matzner, C. D., & Ushomirsky, G. 1997, ApJ, 482, 442
Bouvier, J. 2008, A&A, 489, L53
Bouvier, J., Matt, S. P., Mohanty, S., et al. 2014, in Protostars and Planets VI, eds. H. Beuther, R. S. Klessen, C. P. Dullemond, & T. Henning, 433
Bouvier, J., Lanzafame, A. C., Venuti, L., et al. 2016, A&A, 590, A78
Bouvier, J., Barrado, D., Moraux, E., et al. 2018, A&A, 613, A63
Curtis, J. L., Agüeros, M. A., Mamajek, E. E., Wright, J. T., & Cummings, J. D. 2019, AJ, 158, 77
Denissenkov, P. A. 2010, ApJ, 719, 28
Eggenberger, P., Haemmerlé, L., Meynet, G., & Maeder, A. 2012, A&A, 539, A70
Elliott, P., Bayo, A., Melo, C. H. F., et al. 2014, A&A, 568, A26
Gallet, F., & Bouvier, J. 2015, A&A, 577, A98
Jeffries, R. D. 2014, EAS Publ. Ser., 65, 289
Kaufer, A., Stahl, O., Tubbesing, S., et al. 1999, The Messenger, 95, 8
Kroupa, P., Aarseth, S., & Hurley, J. 2001, MNRAS, 321, 699
Meingast, S., Alves, J., & Fürnkranz, V. 2019, A&A, 622, L13
Messina, S., Lanzafame, A. C., Feiden, G. A., et al. 2016, A&A, 596, A29
Pecaut, M. J., & Mamajek, E. E. 2013, ApJS, 208, 9
Piau, L., & Turck-Chièze, S. 2002, ApJ, 566, 419
Pinsonneault, M. H., Kawaler, S. D., Sofia, S., & Demarque, P. 1989, ApJ, 338, 424
Pinsonneault, M. H., Kawaler, S. D., & Demarque, P. 1990, ApJS, 74, 501
Ratzenböck, S., Meingast, S., Alves, J., Möller, T., & Bomze, I. 2020, A&A, submitted [arXiv:2002.05728]
Ricker, G. R., Winn, J. N., Vanderspek, R., et al. 2015, J. Astron. Tel. Inst. Syst., 1, 014003
Soderblom, D. R., Jones, B. F., Balachandran, S., et al. 1993, AJ, 106, 1059
Somers, G., & Pinsonneault, M. H. 2014, ApJ, 790, 72
Somers, G., & Pinsonneault, M. H. 2015, MNRAS, 449, 4131
Talon, S., & Charbonnel, C. 2005, A&A, 440, 981
Théado, S., & Vauclair, S. 2012, ApJ, 744, 123
Ventura, P., Zeppieri, A., Mazzitelli, I., & D'Antona, F. 1998, A&A, 331, 1011
Zahn, J. P. 1992, A&A, 265, 115